

A Principle of Non-Hermitian Wave Modulators by Indefinitely Small Physical Controls

Youngsun Choi, Yu Sung Choi, Seok Ho Song, Kyungsik Yu, Nimrod Moiseyev, and Jae Woong Yoon*

Interferometers and resonant cavities are indispensable driving mechanisms for compact, high-speed, and low-power modulators and switches in modern signal processing systems. However, their limitations in key performance metrics critically restrict present data-processing capabilities. Here, a completely different wave-modulation mechanism is proposed based on non-Hermitian dynamics near an exceptional point (EP) singularity. The proposed modulator is enabled by EP-bypassing adiabatic processes that exclusively select different final states depending on active trigger signal possibly at indefinitely small magnitude in principle. Importantly, this operation principle does not involve any explicit frequency-dispersive feature in stark contrast to interference or resonance effects. In addition, it can be implemented in available device-engineering platforms such as integrated optical circuits. Therefore, it is of great interest to further investigate the proposed principle for improved signal-processing systems on forthcoming demand.

phase transition,^[2–5] strong direction selectivity,^[6–10] chiral state transfer,^[11,12] and divergent resonance shifts.^[13,14] These phenomena are fundamentally related to self-intersecting Riemann-sheet geometries of complex eigenvalue spectra around an EP.

In particular, time-asymmetric state transfer for dynamically encircling an EP^[15–22] is arguably one of the most exotic non-Hermitian properties originating from the characteristic Riemann-sheet geometries. In this unique non-Hermitian effect, slow adiabatic processes along a closed parametric loop around an EP create robust time-asymmetric state evolution that potentially enables novel device classes.^[20–22] In further studies, the time-asymmetric effect persistently appears even for parametric loops not enclosing an EP^[23] and

1. Introduction

Exceptional point (EP) is a parametric singularity where multiple eigenstates in non-Hermitian coupled wave systems become coalescent and the completeness of corresponding Hilbert space breaks down.^[1] Consequently, EPs produce various anomalous effects including spontaneous symmetry-breaking

for fast Hamiltonian hopping processes beyond the adiabatic limit.^[24] These results suggest that the essential condition for the time-asymmetric final-state selection is not merely the topological inclusion of an EP but the presence of a specific parametric region where the imaginary-eigenvalue Riemann sheets cross each other while the real-eigenvalue Riemann sheets anticross, e.g., the parity-time (PT) symmetric axis in the unbroken-symmetry phase.

Toward this end, we speculate that the time-asymmetric state-transfer effect could be one interesting instance out of wider variety of novel dynamic properties obtainable from the unique Riemann-sheet geometries. Very recently, near-EP adiabatic processes along the PT-symmetric axis show intriguing effects such as stopped light without any coherent nonlinear processes^[25] and robust transmission of spatially coded information in the presence of significant symmetry-breaking power exchange.^[26] Therefore, it is of great interest to further investigate near-EP dynamic effects in search of novel non-Hermitian properties under various control schemes.

In this paper, we propose a near-EP adiabatic-process configuration that enables extremely efficient state modulation without any interference or resonance mechanisms indispensable for conventional approaches.^[27] In the proposed modulation mechanism, we use a slow dynamic return process narrowly bypassing an EP in the adiabatic limit. Such dynamic process selects a different final state depending on the bypass parity with respect to the EP. A complete switching action between two orthogonal

Y. Choi, Y. S. Choi, S. H. Song, J. W. Yoon

Department of Physics

Hanyang University

Seoul 04763, South Korea

E-mail: yoonjw@hanyang.ac.kr

K. Yu

School of Electrical Engineering

Korea Advanced Institute of Science and Technology


Daejeon 34141, South Korea

N. Moiseyev

Schulich Faculty of Chemistry and Faculty of Physics

Technion-Israel Institute of Technology

Haifa 32000, Israel

 The ORCID identification number(s) for the author(s) of this article can be found under <https://doi.org/10.1002/lpor.202200580>

© 2023 The Authors. *Laser & Photonics Reviews* published by Wiley-VCH GmbH. This is an open access article under the terms of the Creative Commons Attribution License, which permits use, distribution and reproduction in any medium, provided the original work is properly cited.

DOI: 10.1002/lpor.202200580

final states and subsequent probability modulation are possibly driven by an indefinitely small change in the bypass parity in principle. We provide essential underlying physics, key optimization parameters, and a potential realization scenario in a photonic integrated circuit platform. Importantly, optical switches and modulators are constituent building blocks in modern signal processing and communication systems and they demand ever-increasing performance measures in terms of power consumption, data rate/bandwidth, and footprint size. In this consideration, the proposed modulation mechanism may significantly improve such performance qualities beyond fundamental limitations in the conventional approaches.

2. Fundamental Theory

We consider a time-varying binary system described by a Schrödinger-type equation

$$\frac{d}{d\tau} |\psi(\tau)\rangle = i\mathbf{H}(\tau) |\psi(\tau)\rangle \quad (1)$$

$$\mathbf{H}(\tau) = \begin{bmatrix} p(\tau) + iq(\tau) & 1 \\ 1 & -p(\tau) - iq(\tau) \end{bmatrix} \quad (2)$$

where τ is relative time to the interstate coupling period. This type of Hamiltonian has been widely studied for PT -symmetric effects,^[2–10] geometric-phase properties,^[11,12] and time-asymmetric processes^[15–22] in association with EP singularities at $p = 0$ and $q = \pm 1$.

The key interest here is to investigate dynamic response $|\psi(\tau)\rangle$ for $\mathbf{H}(\tau)$ under specific conditions that p and q slowly change in time along a segment trajectory very closely bypassing an EP, as schematically illustrated in **Figure 1a**. In this figure, the two bypass trajectories are identical in most of the parts and the only differences are in the close vicinity of the EP. One detours the EP on the left while the other on the right. The question is how much the final states differ if they are evolved from an identical initial state for these two parametric trajectories. In order to describe such two conjugate trajectory cases in a mathematically convenient way, we define a bypass trajectory by a relation as

$$p = f_{sw} B(q) \quad (3)$$

where $B(q)$ is a certain positive function which has nonzero values only in the close vicinity of the EP and f_{sw} is a switching factor which takes $f_{sw} > 0$ for a bypass on the right or $f_{sw} < 0$ for a bypass on the left, as indicated in **Figure 1a**. f_{sw} also can be used to continuously tune the distance of the trajectory from the EP. For a given parametric trajectory due to Equation (3), a slow bypass round-trip process is obtained by appropriately selecting $q(\tau)$ profile over a given time window T , as shown in **Figure 1b**.

According to the standard quantum adiabatic theorem, a dynamic state in a slowly time-varying system in the adiabatic limit predominantly stays in the instantaneous eigen state if the process starts from an eigenstate.^[28] Instantaneous eigenstate is referred to as adiabatic state in general. In our discussion hereafter, $|\psi(\tau)\rangle$ and $|u(\tau)\rangle$ denote the dynamic and adiabatic states, respectively, and we begin our argument on the basis of the standard adiabatic theorem. The adiabatic state $|u_{\pm}(\tau)\rangle$ for a given initial

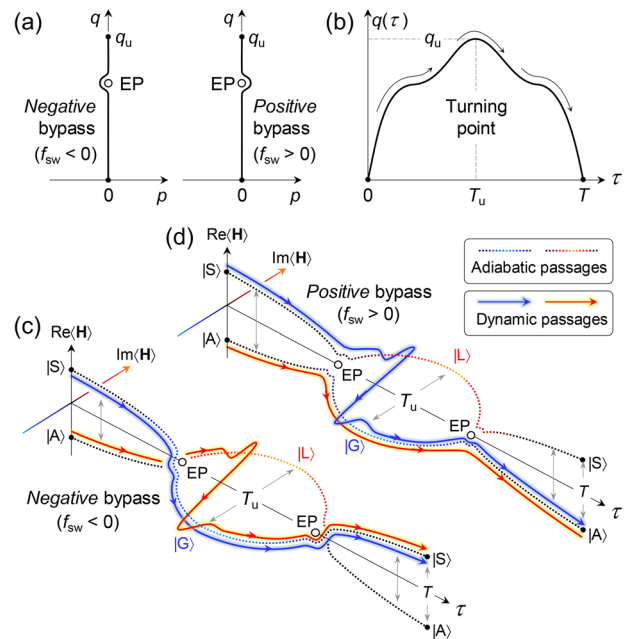


Figure 1. Narrow bypass processes around an exceptional point (EP) for a robust wave switching effect. a) Parametric p - q trajectories bypassing an EP. f_{sw} is the switching factor in Equation (3). b) Example time-dependent profile $q(\tau)$ for a complete EP-bypass roundtrip process. Conceptual illustration of adiabatic and dynamic passages of complex-energy expectation value $\langle \mathbf{H} \rangle$ for c) negative bypass trajectory ($f_{sw} < 0$) and d) positive bypass trajectory ($f_{sw} > 0$). $\langle \mathbf{H} \rangle = \langle \mathbf{H} \rangle_{\psi} = \langle \psi | \mathbf{H} | \psi \rangle$ for dynamic-state passages and $\langle \mathbf{H} \rangle = \langle \mathbf{H} \rangle_u = \langle u | \mathbf{H} | u \rangle$ for adiabatic passages. Therein, $|S\rangle$ and $|A\rangle$ denote the symmetric and antisymmetric modes, respectively, while $|G\rangle$ and $|L\rangle$ represent the gain and loss modes, respectively.

eigenstate is determined by either one of eigenvectors $|E_{\pm}\rangle$ such that its corresponding eigenvalue $E_{\pm} = \pm[1 + (p + iq)^2]^{1/2}$ as well as state-vector itself are continuous along a given p - q trajectory.

A convenient way for describing the adiabatic state characteristics is to see adiabatic expectation-value passage $\langle \mathbf{H} \rangle_u = \langle u | \mathbf{H} | u \rangle$. In **Figure 1c**, we show $\langle \mathbf{H} \rangle_u$ passages (dotted curves) for a negative bypass ($f_{sw} < 0$). We see that $\langle \mathbf{H} \rangle_u$ passage for adiabatic state $|u_+(\tau)\rangle$ from the upper-energy eigenstate $|S\rangle = 2^{-1/2}[1 \ 1]^T$ (symmetric mode) at the starting point ($p = q = 0$) is connected to gain mode $|G\rangle = (2q)^{-1/2}[i\eta^{-1} \ \eta]^T$ around the turning point at $\tau = T_u$ where the system stays in the broken PT -symmetry phase, i.e., $q(T_u) > 1$ and $p(T_u) \approx 0$. Here, $\eta = [q + (q^2 - 1)^{1/2}]^{1/2}$ which is greater than 1 in the broken PT -symmetry phase.

$\langle \mathbf{H} \rangle_u$ passage for another adiabatic state $|u_-(\tau)\rangle$ evolved from the lower-energy eigenstate $|A\rangle = 2^{-1/2}[1 \ -1]^T$ (antisymmetric mode) at the starting point is connected to loss mode $|L\rangle = (2q)^{-1/2}[i\eta \ \eta^{-1}]^T$ around the turning point at $\tau = T_u$ in the broken PT -symmetry phase. Therefore, the adiabatic states for a negative bypass process ($f_{sw} < 0$) are characterized by two different courses $\{|u_+(f_{sw} < 0)\rangle: |S\rangle \rightarrow |G\rangle \rightarrow |S\rangle\}$ and $\{|u_-(f_{sw} < 0)\rangle: |A\rangle \rightarrow |L\rangle \rightarrow |A\rangle\}$.

In contrast, the adiabatic states in positive bypass processes ($f_{sw} > 0$) take completely opposite courses $\{|u_+(f_{sw} > 0)\rangle: |S\rangle \rightarrow |L\rangle \rightarrow |S\rangle\}$ and $\{|u_-(f_{sw} > 0)\rangle: |A\rangle \rightarrow |G\rangle \rightarrow |A\rangle\}$, as shown in **Figure 1d**. This f_{sw} -dependent adiabatic-state switching effect is an essential consequence of the proximity of the EP as a modal

branch point and the inherent antisymmetry in the imaginary-eigenvalue splitting with respect to p such that (double signs in same order)

$$E_{\pm}(|p| \ll 1, q \approx 1) \approx \begin{cases} \pm |p|^{1/2}(1+i) & \text{for } p > 0 \\ \pm |p|^{1/2}(1-i) & \text{for } p < 0 \end{cases} \quad (4)$$

Dynamic state $|\psi(\tau)\rangle$ evolution can be readily predicted once $|\mathbf{u}_{\pm}(f_{\text{sw}})\rangle$ is determined. In contrast to the conventional Hermitian cases, $|\psi(\tau)\rangle$ for a non-Hermitian \mathbf{H} does not always follow the adiabatic state because gain mode $|G\rangle$ exclusively overtakes system's response in the strong imaginary-splitting regime, regardless of any selected initial state.^[15–21] In our case, $|\psi(\tau)\rangle$ in $|\mathbf{u}_{-}(f_{\text{sw}} < 0)\rangle$ or $|\mathbf{u}_{+}(f_{\text{sw}} > 0)\rangle$ is unstable as these adiabatic states involve loss mode $|L\rangle$ around the turning point in the broken PT -symmetry phase. $|\psi(\tau)\rangle$ transiently staying in such unstable adiabatic states undergoes an antiadiabatic jump toward the other adiabatic state $|\mathbf{u}_{+}(f_{\text{sw}} < 0)\rangle$ or $|\mathbf{u}_{-}(f_{\text{sw}} > 0)\rangle$ involving $|G\rangle$ and finally ends up in the corresponding adiabatic final state $|\mathbf{u}_{+}(f_{\text{sw}} < 0)\rangle = |S\rangle$ or $|\mathbf{u}_{-}(f_{\text{sw}} > 0)\rangle = |A\rangle$ at $\tau = T$ as an exclusively preferred final dynamic state depending on f_{sw} .

Intriguingly, switching of the preferred final state in EP-bypass processes in the adiabatic limit depends only on the sign of switching factor f_{sw} in principle, not explicitly on its absolute magnitude. Note that connection of the adiabatic states to the gain and loss modes does not change as far as f_{sw} keeps its sign. Therefore, this state switching mechanism is potentially available even with an indefinitely small physical change that flips the sign of f_{sw} around a certain critical condition.

The EP-bypass process and associated switching effect may seem similar to the EP-encirclement process in our previous work^[17,18] because they both involve a common essential physics—antiadiabatic jump from the loss mode to the gain mode. Nevertheless, the two process configurations are distinguished from each other in their resultant actions. First, the action is time-symmetric in the EP-bypass process while it is time-asymmetric in the EP-encirclement process. In other words, the preferred final states for the forward and backward time directions are identical in the EP-bypass process whereas they are totally different from each other in the EP-encirclement process. Second, the state flip between the initial and final states happens in the opposite conditions for the two process configurations. The dynamic state in the EP-bypass process flips whenever the antiadiabatic jump is involved. In contrast, the dynamic state in the EP-encirclement process flips whenever the state evolves in a totally adiabatic manner during the entire process. Most importantly, the EP-encirclement process in the previous study is hardly applicable by itself alone for any efficient state-switching or modulation mechanism because it demands time-reversal of the entire process, which seems uneasy if there is no additional switch that exchanges the input and output ports. However, the EP-encirclement process might provide an efficient state-switching mechanism if the parametric loop is very close to the EP so that the encircling direction is switchable with certain small physical stimuli. We consider that this is an interesting subject for follow-up study in the future.

3. Numerical Analysis on the Key Effects

In further quantitative study on the proposed concept, an important issue is to appropriately configure speed $V = d(p + iq)/d\tau$ of parametric change such that the process keeps nonadiabatic transition from the stable to the unstable adiabatic state as low as possible over the entire process. This problem is related to the standard adiabatic condition^[17,28]

$$\left| \langle \mathbf{u}_{+}^* | d\mathbf{H}/d\tau | \mathbf{u}_{-} \rangle \right| \approx |V| \ll |E_{+} - E_{-}|^2 \quad (5)$$

in our case. Equation (5) implies that the speed of parametric change should be considerably low ($|V| \approx 0$) near the EP where $|E_{+} - E_{-}| \approx 0$. Therefore, it is reasonable to take V as a function of $\Delta E = E_{+} - E_{-}$ on the reference trajectory $p_{\text{ref}}(\tau) = B(q(\tau))$, rather than as a certain arbitrary function of τ , which should be subject to random numerical optimization. Among a wide variety of possible functional forms, we take a simple trial form as

$$|V| = V_{\text{avg}} N_v |\Delta E|^J \quad (6)$$

where V_{avg} is average speed, J is speed-profile order, and N_v is a normalization constant for a relation $V_{\text{avg}} = 2L_{\text{ref}}/T$ with L_{ref} denoting segment path length of the reference bypass trajectory on p - q plane. We use speed-profile order J as an optimization parameter for maximizing the state-switching effect for given trajectory $B(q)$ and process time T .

In addition, we assume a reference bypass trajectory

$$B(0 \leq q \leq q_u) = B_0 \theta [2(q - q_1)/w] \theta [2(q_2 - q)/w] \quad (7)$$

where $\theta(x)$ is a Gaussian unit-step function

$$\theta(x) = \frac{1}{\sqrt{\pi}} \int_{-\infty}^x \exp(-\xi^2) d\xi \quad (8)$$

q_1 and q_2 are bypass range bounds and w is bypass ramp width. We use the classical Runge–Kutta (RK4) method to numerically solve Equation (1) under these conditions.

Numerically demonstrating the proposed switching effect, we take a trial case with $B_0 = w = 0.01$, $q_1 = 0.99$, $q_2 = 1.01$, and $q_u = 1.4$. The negative ($f_{\text{sw}} = -1$) and positive ($f_{\text{sw}} = +1$) bypass trajectories in this case are almost identical and the slight difference is only in a tiny region ($0.99 < q < 1.01$) around the EP, as shown in **Figure 2a**. We calculate dynamic state $|\psi\rangle$ for a sufficiently large process time at $T = 100$ and an optimal speed-profile order at $J = 1.5$. The results are summarized in **Figure 2b,c** for $f_{\text{sw}} = -1$ and $+1$, where dynamic expectation-value $\langle \mathbf{H} \rangle_{\psi}$ passages as functions of q are indicated in comparison with the adiabatic expectation-value $\langle \mathbf{H} \rangle_u$ passages. Therein, we confirm that final dynamic state $|\psi(T; f_{\text{sw}} < 0)\rangle \approx |S\rangle$ whereas $|\psi(T; f_{\text{sw}} > 0)\rangle \approx |A\rangle$ regardless of the initial-state selection, as predicted previously. Remarkably, extinction ratio $r_{\text{ext}} = |\langle S | \psi(T; f_{\text{sw}} = -1) \rangle|^2 / |\langle S | \psi(T; f_{\text{sw}} = +1) \rangle|^2$ of the symmetric-state probabilities in the final states is 2.3×10^4 (43.6 dB) for this trial case with extremely narrow EP-bypass trajectories.

Modulation characteristics under continuous switching factor f_{sw} control in this trial case are shown in **Figure 3a**, where we

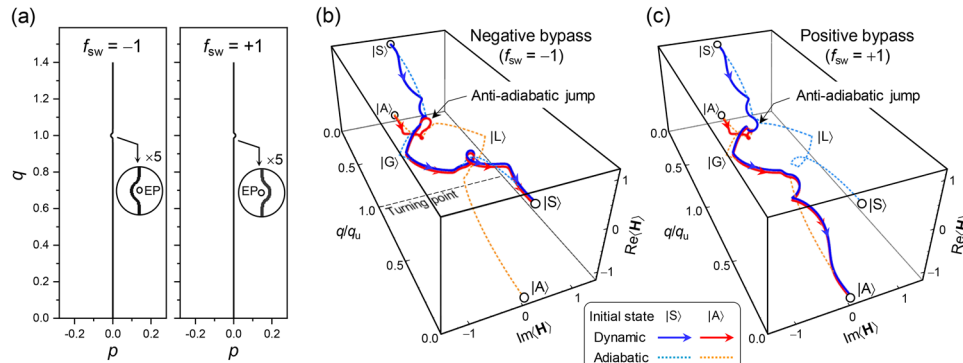


Figure 2. State-witching effect for very narrow EP-bypass processes. a) Trial reference bypass trajectories for $f_{sw} = \pm 1$. Parameters for the reference bypass trajectory function in Equation (7) are $q_1 = 0.99$, $q_2 = 1.01$, $q_u = 1.4$, $w = 0.01$, and $B_0 = 0.01$. Circular insets show magnified ($\times 5$) views of the trajectories near the EP at $p = 0$ and $q = 1$. Dynamic-state passages of $\langle \mathbf{H} \rangle_\psi$ for b) a negative bypass ($f_{sw} = -1$) and c) a positive bypass ($f_{sw} = +1$) in comparison with the adiabatic-state passages of $\langle \mathbf{H} \rangle_u$. We assume $|\psi(0)\rangle = |S\rangle$ or $|A\rangle$, $T = 100$, and $J = 1.5$.

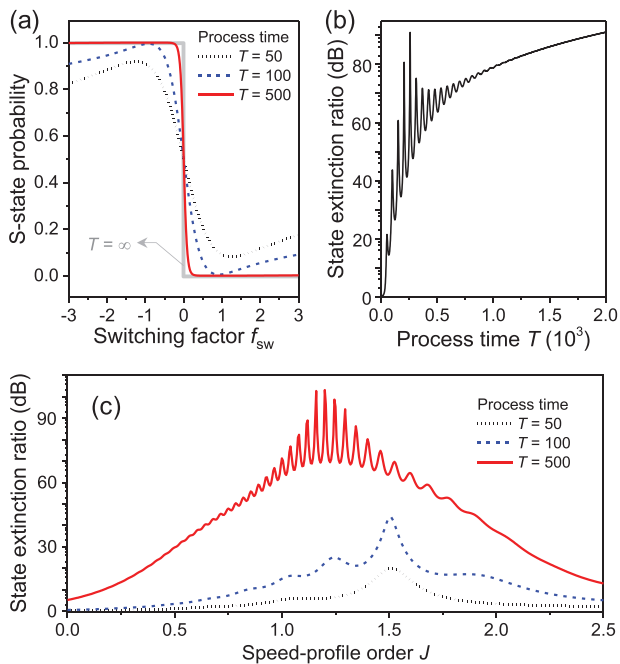


Figure 3. Switching performance for the trial bypass trajectories in Figure 2a. a) Probability P_S of finding final state $|\psi(T)\rangle$ in symmetric eigenstate $|S\rangle$ as a function of switching factor f_{sw} for $T = 50$, 100 , and 500 . b) Dependence of extinction ratio r_{ext} on process time T for $J = 1.5$. Here, $r_{ext} = |\langle S|\psi(T; f_{sw} = -1)\rangle|^2 / |\langle S|\psi(T; f_{sw} = +1)\rangle|^2$, indicating a ratio of symmetric-state probability for the negative bypass to that for the positive bypass. c) Dependence of extinction ratio r_{ext} on speed-profile order J for $T = 50$, 100 , and 500 .

present f_{sw} -dependent symmetric-state probability $P_S = |\langle S|\psi\rangle|^2 / |\langle \psi|\psi\rangle|^{-1}$ in the final state. In the ideal adiabatic limit ($T \rightarrow \infty$), $P_S(f_{sw})$ represents a step function taking 1 for $f_{sw} < 0$ or 0 for $f_{sw} > 0$. The step-like switching profile is persistent even in a non-ideal condition for $T = 500$ in this trial case. Therefore, the proposed concept is arguably capable of producing a high-extinction modulation triggered by indefinitely small physical controls on f_{sw} as far as it secures the adiabatic condition over the entire process.

As process time T decreases, step-like profile of $P_S(f_{sw})$ gradually turns into a continuous function with a maximum in the negative f_{sw} domain and a minimum in the positive f_{sw} domain. This characteristic profile-shape dependence is understood that the state-switching effect disappears for $|f_{sw}| \gg 1$ or $T \rightarrow 0$ as the adiabatic condition in Equation (5) is no longer sustainable for large bypass trajectories or for small process time. In such nonadiabatic limit, probability distribution over the two eigenstates gets even, i.e., $P_S \rightarrow 1/2$, because the coalescent singular eigenstate at the EP yields identical projections onto the two independent adiabatic states.

Dependence of state extinction ratio $r_{ext} = |\langle S|\psi(T; f_{sw} = -1)\rangle|^2 / |\langle S|\psi(T; f_{sw} = +1)\rangle|^2$ on process time T reveals the modulation performance in greater details for the adiabatic, nonadiabatic, and their intermediate domains, as shown in Figure 3b. In the highly adiabatic limit for $T > 1000$, r_{ext} monotonically increases with T in the large value region beyond 10^7 (70 dB). In the nonadiabatic limit for $T < 50$, r_{ext} quickly approaches 1 (0 dB) at $T = 0$ as explained previously. In the intermediate domain ($50 < T < 1000$), the dependence of r_{ext} on T shows two major features: Rapid growth toward the adiabatic-limit dependence and periodic peaks. These peaks in r_{ext} appear with a period $\Delta T \approx 55$ and are related to periodic minima of the symmetric-state probability in the final state for $f_{sw} = +1$, i.e., $|\langle S|\psi(T; f_{sw} = +1)\rangle|^2 \approx 0$ resulting in diverging r_{ext} .

In particular, $|\psi(\tau; f_{sw} = +1)\rangle$ after the antiadiabatic jump dominantly evolves along a stable adiabatic state ending up in antisymmetric eigenstate $|A\rangle$ at $\tau = T$, implying $|\psi(T; f_{sw} = +1)\rangle \approx |A\rangle$ and thereby $|\langle S|\psi(T; f_{sw} = +1)\rangle|^2 \approx 0$ in the adiabatic limit. However, the state evolution under intermediately adiabatic conditions yields non-negligible projection onto the instable adiabatic state ending up in symmetric eigenstate $|S\rangle$ at $\tau = T$. Magnitude of this projection at the end of the process is described by nonadiabatic transition amplitude^[17]

$$C \approx \int_0^T \frac{\langle u_-^* | d\mathbf{H}/d\tau | u_+ \rangle}{E_+(\tau) - E_-(\tau)} \exp \left[-i \int_\tau^T \Delta E(t) dt \right] d\tau \quad (9)$$

in our case. The key factor associated with the periodic maxima in $r_{ext}(T)$ is the exponential term in the integrand of Equation (9).

This term describes oscillation of instantaneous nonadiabatic transition at time τ . Note that ΔE is predominantly real-valued toward the end of the process for which the system stays on the PT -symmetric axis in the unbroken-symmetry phase. Therefore, the exponential term in the integrand represents oscillation. Superposition of the instantaneous nonadiabatic transition amplitudes at the end of the process results in interference-like periodic fringe in C over process time T domain and the minima in this fringe produce sharp periodic spikes in r_{ext} .

Associated with the nonadiabatic transition which should be minimized for stronger modulation effect, speed-profile order J in Equation (6) is a key optimization parameter for given reference trajectory function $B(q)$ and process time T . For $J = 0$, speed $|V| = |d(p + iq)/d\tau|$ of parametric change is constant at average speed V_{avg} over the entire process. As J increases, the parametric change slows down from V_{avg} near the EP where $\Delta E \approx 0$ while it speeds up beyond V_{avg} otherwise. J tunes this speed-adjustment condition depending on the magnitude of ΔE . In the highly adiabatic limit, the optimal J for strongest modulation effect must be close to 1 because it conforms the standard adiabatic condition in Equation (5). In contrast, optimal J in the intermediately adiabatic domain might be substantially deviated from 1 due to non-negligible nonadiabatic transition amplitudes and their intricate superposition effects. In Figure 3c, we show the dependence of r_{ext} on J for several selected T values. The optimal J for given T is ≈ 1.5 for $T = 50$ and 100 in the intermediately adiabatic domain and it shifts toward 1 for $T = 1000$ in the highly adiabatic limit. The periodic maxima are again due to the interference-like fringe in nonadiabatic transition amplitude C .

4. Potential Realization on an Integrated-Optics Platform

The proposed modulation principle can be favorably implemented in a photonic integrated-circuit platform. Guided photonic modes in a coupled waveguide structure follows the dynamics due to Equation (1) with parametric relations $\tau = \kappa z$, $p = \text{Re}(\Delta n_{\text{eff}}) (2\kappa)^{-1} k_0$, and $q = \text{Im}(\Delta n_{\text{eff}}) (2\kappa)^{-1} k_0$, where z is position along the waveguide transmission axis, κ is interchannel coupling constant, Δn_{eff} is complex effective-index difference between the two waveguide channels, and k_0 is vacuum wavenumber.^[17,18] With these parametric relations, we can estimate magnitudes of real physical parameters required for the proposed effect. The interchannel coupling constant is a key scaling factor and it is given by $\kappa = \pi b^{-1}$, where b is beat length, which is typically in the order of $10 \mu\text{m}$ in the telecommunications bands around wavelength $\lambda = 1.5 \mu\text{m}$ for group IV or III-V semiconductor structures. Subsequent conversion between the normalized and real physical parameters is footprint length $L = \kappa^{-1} T \approx 3.3 \times T \mu\text{m}$, depth of the dynamic refractive-index modulation $\text{Re}(\Delta n_{\text{eff}}) = 2\kappa k_0^{-1} \Delta p \approx 0.15 \times \Delta p$, the maximal difference of imaginary effective index $\text{Im}(\Delta n_{\text{eff}}) = 2\kappa k_0^{-1} q_u \approx 0.15 \times q_u$. For the trial case in Figure 3 with $T = 100$, $\Delta p = 0.02$, and $q_u = 1.4$ in Figure 3, conversion to the real physical parameters yields $L \approx 330 \mu\text{m}$, $\text{Re}(\Delta n_{\text{eff}}) \approx 3 \times 10^{-3}$, and $\text{Im}(\Delta n_{\text{eff}}) \approx 0.21$. These values are favorably acceptable in practical structures. Even in cases where certain experimental restrictions require substantially smaller parameter values, there are still much

room for further parametric optimization of reference path $B(q)$ and speed profile $V(\tau)$ for given required Δp , q_u , and T values.

We note that q is determined by the imaginary-part difference of the effective indices for the two waveguide channels and it does not necessarily require balanced gain and loss in principle. This property is based on the gauge invariance of the key non-Hermitian dynamics. A generic coupled-mode equation for a binary waveguide system can be written as

$$\frac{d}{dz} \begin{bmatrix} a_1 \\ a_2 \end{bmatrix} = i \begin{bmatrix} n_1 k_0 & \kappa \\ \kappa & n_2 k_0 \end{bmatrix} \begin{bmatrix} a_1 \\ a_2 \end{bmatrix} \quad (10)$$

where a_j and n_j are amplitude and effective index of the guided mode at waveguide channel j , respectively. Taking a gauge transformation such that

$$a_j \rightarrow a_j \exp(in_a k_0 z - \gamma_a z) \quad (11)$$

where $n_a = \text{Re}(n_1 + n_2)/2$ is the average effective index and $\gamma_a = k_0 \text{Im}(n_1 + n_2)/2$ is the average attenuation constant, common changes in the magnitudes and phase retardations at the two waveguide channels are eliminated in the dynamics description and the coupled mode equation in Equation (10) reduces to Equation (1) with the parametric mapping of $\tau = \kappa z$, $p = \text{Re}(\Delta n_{\text{eff}}) (2\kappa)^{-1} k_0$, $q = \text{Im}(\Delta n_{\text{eff}}) (2\kappa)^{-1} k_0$, and $\Delta n_{\text{eff}} = n_2 - n_1$. This implies that the desired non-Hermitian dynamics is fully obtainable in the absence of the perfect balance between gain and loss, i.e., $\text{Im}(n_1 + n_2) = 0$ and $\gamma_a = 0$, as long as the common attenuation ($\gamma_a > 0$) or amplification ($\gamma_a < 0$) is in acceptable levels for given measurement conditions, as previously demonstrated by many experimental works in the literature.^[8,18,24,29,30] For non-Hermitian systems involving resonant cavities, however, very small amount of gain-loss imbalance might be seriously detrimental to the experimental observability because effects of the common attenuation or amplification are greatly enhanced by factors in the order of resonance quality factor.^[13,14,31,32] In our case based on nonresonant elements, the gain-loss balance condition is not strictly required. Therefore, the desired time-varying non-Hermitian Hamiltonian can be synthetically constructed by appropriately configuring Δn_{eff} along propagation axis z , as previously established using various index-control schemes with state-of-the-art thin-film deposition and nanolithography techniques.

Particularly for potential photonic modulators or switches based on the adiabatic EP-bypass processes, active control mechanism for $p(z)$ is crucial for driving the bypass-parity change and it can be conveniently obtained using various electro-optic (EO) effects available in practice.^[27,33,34] For example, the free-carrier plasma effect in III-V compound semiconductor media produces $\text{Re}(\Delta n_{\text{eff}}) \approx 10^{-2}$ for carrier density change in the order of 10^{18} cm^{-3} ,^[34] which is obtainable by applying electrical bias voltage or current across a pn or pin junction along the waveguide core axis.

In Figure 4a, we schematically illustrate a coupled-waveguide electro-optic modulator under such a control scheme. A single-mode waveguide at the input splits into two channels to form a binary non-Hermitian system where the desired EP-bypass processes happen. The two waveguide channels merge at the output single-mode waveguide so that a symmetric part of the final state freely transmits through, while its antisymmetric part is totally

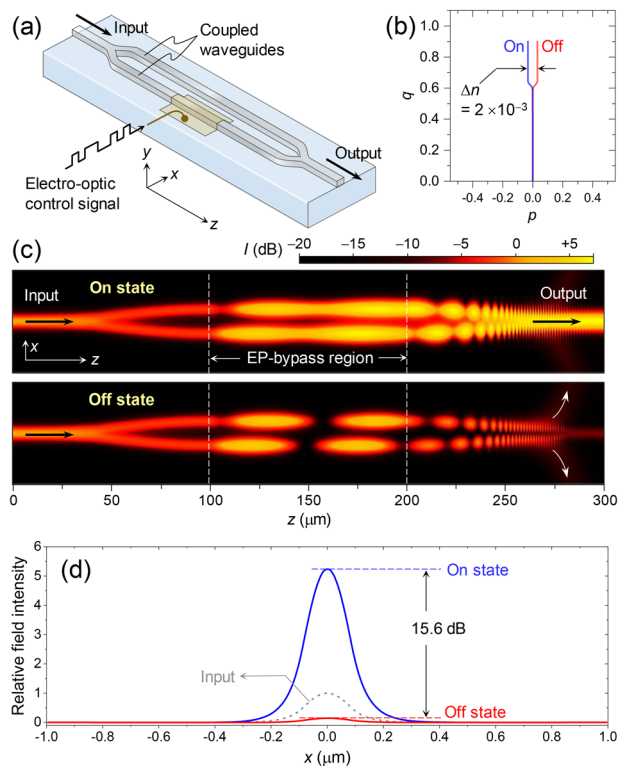


Figure 4. Potential realization in an optical waveguide structure. a) Schematic of an EP-bypass waveguide modulator with an electro-optic tuning mechanism for bypass-parity control. b) Bypass trajectories for on and off states of a trial waveguide structure. c) Optical transmission through a trial waveguide structure for the on and off states at wavelength 1550 nm. The effective-index profiles for the on and off state follow the on and off trajectories in (b), respectively. In this calculation, we assume InGaAs core (refractive index 3.53), SiO₂ clad (refractive index 1.444), and speed-profile order $J = 4$. Here, we apply identical gain and loss at 2189 cm⁻¹ in the upper and lower channels, respectively. d) Transmitted output intensity profiles for the on and off states in comparison with the input intensity profile.

rejected. The bypass-parity change is driven by an electro-optic control signal injected at one channel.

Assuming this device configuration in an InGaAs-core and SiO₂-clad structure, we numerically demonstrate a decent power-modulation operation as shown in Figure 4b–d. We apply on and off bypass trajectories in Figure 4b to a pair of InGaAs slab waveguides with core width 180 nm, interchannel gap 300 nm, and footprint length 100 μm . Switching between these on and off bypass trajectories are induced by refractive index change $\Delta n = 2 \times 10^{-3}$ in the InGaAs core at one waveguide channel. Figure 4c shows transmission of near-infrared light at 1550 nm wavelength and transverse-magnetic polarization (electric field normal to the paper plane) for the on and off bypass trajectories. We see a strong amplified transmission at the output for the on state and a weak attenuated transmission for the off state. We note that absolute output power values for the on and off states are variable with the modal gain constant but their ratio is independent. Intensity ratio between the on and off output states, i.e., on/off extinction ratio, is 15.6 dB in this calculation. In comparison, a Mach–Zehnder interferometer (MZI) structure with identical index change, core width, and footprint length yields a substantially lower extinction

ratio ≈ 3.2 dB for an operation around the maximal on-state efficiency point.

In this MZI structure, the refractive index change required for the complete output extinction with π phase difference between the two waveguide arms is $\Delta n_\pi = 3.89 \times 10^{-3}$ which is 1.9 times larger than given $\Delta n = 2 \times 10^{-3}$, resulting in the lower extinction ratio when we assume the waveguide design and refractive index change identical to the EP-bypass structure. Although the MZI structure might be further optimized for better performance, it should be quite challenging to make it surpass our proposed structure without increasing its footprint length and index change. The only way is to reduce Δn_π by a factor below 1/1.9 and this requires enhanced core-confinement factor Γ of the guided mode by a factor above 1.9. The enhanced core-confinement factor to the required level may be obtained by increasing the core width. However, it is impossible in our particular case because the core-confinement factor in our simulated case is 0.78 and its enhancement by a factor of 1.9 yields $\Gamma \approx 1.48$, which substantially exceeds the theoretical limit of $\Gamma < 1$ for physically conceivable waveguide designs. Therefore, the EP-bypass approach considerably alleviates technical issues associated with unfavorable trade-off between the on/off extinction ratio and device-footprint length in the conventional interferometer-based approaches.

Importantly, the device-footprint length is directly related to modulation speed limit which is imposed by resistance-capacitance (RC) time constant involved in EO signal-injection electronics. Although the exact speed-limit value depends on EO effect types and detailed structure geometries, shorter device yields a smaller RC-time constant and, thereby, higher speed limit in general. Considering that 100 Gbit s⁻¹ data rate is obtainable with a 1 mm long MZI using a depletion-based free-carrier EO effect phase shifter,^[35] our numerical result with a 0.1 mm long device suggests a potential Tbit/s-level data rate in a high-extinction regime around 15 dB, which is remarkably higher from the marginally acceptable 3 dB convention.

Although the speed limit in the index change is a crucial factor, precise estimation of the modulation speed limit requires time-domain electromagnetic analyses for given spatiotemporal profiles of presumable dynamic change in the refractive index. The direct time-domain analyses basically requires separate numerical calculations independent of the frequency-domain spatial-mode analyses based on Equation (10). Note that time τ in Equation (1) is mapped onto position z along the optical axis of the waveguide system in Equation (10) which is formulated from the frequency-domain Maxwell's equations. Nevertheless, the frequency-domain solutions due to Equation (10) can be used for time-domain analyses by means of the Fourier transformation. In the Fourier-transformation-based time-domain analyses, time-varying dielectric-constant distribution is decomposed into spectral amplitudes $\epsilon(\omega)$, frequency dependent effective index $n_e(\omega)$ and coupling constant $\kappa(\omega)$ are calculated for given $\epsilon(\omega)$, the spectral amplitudes of the output at each sampled frequency is calculated based on Equation (10), and the inverse Fourier transformation of the output spectral amplitudes finally yields the output amplitude solution in the time domain.

In this respect, spectral bandwidth $\Delta\nu$ of remarkable on/off extinction ratio conveniently provides a reasonable estimation of the maximally achievable limit of the modulation speed. Although detailed information on the generated pulse properties

are obtainable from the Fourier-transform-based time-domain analyses, a simple bandwidth calculation should provide a reasonable estimation as far as we only concern modulation speed limit. We numerically estimate 3 dB bandwidth $\Delta\lambda_{3\text{-dB}}$, a wavelength range that sustains extinction ratio exceeding 3 dB, as conventionally used. In our simulated case, $\Delta\lambda_{3\text{-dB}} \approx 90$ nm and corresponding frequency bandwidth $\Delta\nu_{3\text{-dB}} \approx 11$ THz. This value implies a speed limit for 3 dB modulation ≈ 11 THz that can be supported by the proposed effect. We note in the state-of-the-art MZI modulator technologies on the LiNbO₃ and semiconductor photonic platforms^[36] that RC-time-constant-limited 3 dB bandwidth of electro-optic index modulation is below 100 GHz and our obtained $\Delta\nu_{3\text{-dB}}$ due to the EP-bypass effect for this trial design is well beyond that level. In another consideration, $\Delta\lambda_{3\text{-dB}} \approx 90$ nm is substantially narrower than one may expect from the interference-free adiabatic processes. This is because speed of the parametric change is too fast and the coupled guided mode evolves in a poorly adiabatic condition in this specific case. The process time parameter $T = 12.1$ in this case and this is substantially smaller than 1000 for highly adiabatic cases in Figure 3b. Therefore, one can readily increase $\Delta\lambda_{3\text{-dB}}$ by increasing device footprint length. In our additional calculation for identical structure with footprint length 500 μm , we confirm $\Delta\lambda_{3\text{-dB}} > 430$ nm and the corresponding spectral band covers the entire optical telecommunications band from 1250 to 1680 nm. In addition, $\Delta\nu_{3\text{-dB}} \approx 54$ THz for this longer footprint design. This improvement favorably involves an additional enhancement of the peak extinction ratio up to 57 dB as a result of improved adiabaticity in the parametric change.

5. Conclusion

We have developed a wave-modulation principle based on adiabatic processes in the vicinity of an EP. For slow adiabatic return processes along a parametric trajectory narrowly bypassing an EP, the final state flips between two orthogonal states in response to the bypass-parity change that is possibly excited even by arbitrarily small physical stimuli. This state-switching effect originates from the stability flip in a binary non-Hermitian eigen-system across an EP and does not rely on interference or resonance excitations which are key operation principles of conventional switches and modulators. Application of this effect to a semiconductor coupled-waveguide structure have theoretically shown practical feasibility for creating highly compact electro-optic modulators of which performance might go beyond the previous limitations. Therefore, it is of our great interest to further study in both theory and experiments for optimal device designs and optoelectronic control architectures in pursuit of Tbit/s-level signal-processing systems on forthcoming demand. In addition, we hope that our results may motivate more extensive research on dynamic non-Hermitian properties and their device applications, taking advantages of their characteristic features from enhanced degrees of control freedom and relaxed physical constraints.

Acknowledgements

This research was supported by the Leader Researcher Program (NRF-2019R1A3B2068083), the Basic Science Research Program (NRF-

2018R1A2B3002539), and the research fund of Hanyang University (HY-202000000000513).

Conflict of Interest

The authors declare no conflict of interest.

Data Availability Statement

The data that support the findings of this study are available from the corresponding author upon reasonable request.

Keywords

adiabatic processes, exceptional points, non-Hermitian Hamiltonians, optical waveguides

Received: August 2, 2022

Revised: March 16, 2023

Published online:

- [1] W. D. Heiss, *J. Phys. A: Math. Theor.* **2012**, *45*, 444016.
- [2] C. M. Bender, S. Boettcher, *Phys. Rev. Lett.* **1998**, *80*, 5243.
- [3] S. Klaiman, N. Moiseyev, U. Günther, *Phys. Rev. Lett.* **2008**, *101*, 080402.
- [4] L. Feng, Z. J. Wong, R. M. Ma, Y. Wang, X. Zhang, *Science* **2014**, *34*, 972.
- [5] Y. Wu, W. Liu, J. Geng, X. Song, X. Ye, C. K. Duan, X. Rong, J. Du, *Science* **2019**, *364*, 878.
- [6] P. Miao, Z. Zhang, J. Sun, W. Walasik, S. Longhi, N. M. Litchinitser, L. Feng, *Science* **2016**, *353*, 464.
- [7] C. Hahn, Y. Choi, J. W. Yoon, S. H. Song, C. H. Oh, P. Berini, *Nat. Commun.* **2016**, *7*, 12201.
- [8] L. Feng, Y. L. Xu, W. S. Fegadolli, M. H. Lu, J. E. B. Oliveira, V. R. Almeida, Y. F. Chen, A. Scherer, *Nat. Mater.* **2013**, *12*, 108.
- [9] Z. Lin, H. Ramezani, T. Eichelkraut, T. Kottos, H. Cao, D. N. Christodoulides, *Phys. Rev. Lett.* **2011**, *106*, 213901.
- [10] R. Fleury, D. Sounas, A. Alù, *Nat. Commun.* **2015**, *6*, 5905.
- [11] C. Dembowski, B. Dietz, H. D. Gräf, H. L. Harney, A. Heine, W. D. Heiss, A. Richter, *Phys. Rev. Lett.* **2003**, *90*, 034101.
- [12] T. Gao, E. Estrecho, K. Y. Bliokh, T. C. H. Liew, M. D. Fraser, S. Brodbeck, M. Kamp, C. Schneider, S. Höfling, Y. Yamamoto, F. Nori, Y. S. Kivshar, A. G. Truscott, R. G. Dall, E. A. Ostrovskaya, *Nature* **2015**, *526*, 554.
- [13] H. Hodaie, A. U. Hassan, S. Wittek, H. G. Gracia, R. E. Ganainy, D. N. Christodoulides, M. Khajavikhan, *Nature* **2017**, *548*, 187.
- [14] W. Chen, Ş. K. Özdemir, G. Zhao, J. Wiersig, L. Yang, *Nature* **2017**, *548*, 192.
- [15] R. Uzdin, A. Mailybaev, N. Moiseyev, *J. Phys. A: Math. Theor.* **2011**, *44*, 435302.
- [16] H. Xu, D. Mason, L. Jiang, J. G. E. Harris, *Nature* **2016**, *537*, 80.
- [17] Y. Choi, C. Hahn, J. W. Yoon, S. H. Song, P. Berini, *Nat. Commun.* **2017**, *8*, 14154.
- [18] J. W. Yoon, Y. Choi, C. Hahn, G. Kim, S. H. Hong, K. Y. Yang, J. Y. Lee, Y. Kim, C. S. Lee, J. K. Shin, H. S. Lee, P. Berini, *Nature* **2018**, *562*, 86.
- [19] Y. Choi, J. W. Yoon, J. H. Hong, Y. Ryu, S. H. Song, *Commun. Phys.* **2020**, *3*, 140.
- [20] I. Gilary, N. Moiseyev, *J. Phys. B: At. Mol. Opt. Phys.* **2012**, *45*, 051002.
- [21] J. Doppler, A. A. Mailybaev, J. Böhm, U. Kuhl, A. Girschik, F. Libisch, T. J. Milburn, P. Rabl, N. Moiseyev, S. Rotter, *Nature* **2016**, *537*, 76.

- [22] A. U. Hassan, B. Zhen, M. Soljačić, M. Khajavikhan, D. N. Christodoulides, *Phys. Rev. Lett.* **2017**, *118*, 093002.
- [23] A. U. Hassan, G. L. Galmiche, G. Harari, P. LiKamWa, M. Khajavikhan, M. Segev, D. N. Christodoulides, *Phys. Rev. A* **2017**, *96*, 052129.
- [24] A. Li, J. Dong, J. Wang, Z. Cheng, J. S. Ho, D. Zhang, J. Wen, X. L. Zhang, C. T. Chan, A. Alù, C. W. Qiu, L. Chen, *Phys. Rev. Lett.* **2020**, *125*, 187403.
- [25] Y. Goldzak, A. A. Mailybaev, N. Moiseyev, *Phys. Rev. Lett.* **2018**, *120*, 013901.
- [26] N. Moiseyev, M. Šindelka, *Phys. Rev. A* **2021**, *103*, 033518.
- [27] G. T. Reed, G. Mashanovich, F. Y. Gardes, D. J. Thomson, *Nat. Photonics* **2010**, *4*, 518.
- [28] Z. Wu, H. Yang, *Phys. Rev. A* **2005**, *72*, 012114.
- [29] S. Weimann, M. Kremer, Y. Plotnik, Y. Lumer, S. Nolte, K. G. Makris, M. Segev, M. C. Rechtsman, A. Szameit, *Nat. Mater.* **2017**, *16*, 433.
- [30] X. Shu, A. Li, G. Hu, J. Wang, A. Alù, L. Chen, *Nat. Commun.* **2022**, *13*, 2123.
- [31] B. Peng, S. K. Özdemir, F. Kei, F. Monifi, M. Gianfreda, G. L. Long, S. Fan, F. Nori, C. M. Bender, L. Yang, *Nat. Phys.* **2014**, *10*, 394.
- [32] L. Chang, X. Jiang, S. Hua, C. Yang, J. Wen, L. Jiang, G. Li, G. Wang, M. Xiao, *Nat. Photonics* **2014**, *8*, 524.
- [33] A. Boes, B. Corcoran, L. Chang, J. Bowers, A. Mitchell, *Laser Photonics Rev.* **2018**, *12*, 1700256.
- [34] B. R. Bennett, R. A. Soref, J. A. Del Alamo, *IEEE J. Quantum Electron.* **1990**, *26*, 113.
- [35] A. Rahim, A. Hermans, B. Wohlfeil, D. Petousi, B. Kuyken, D. V. Thourhout, R. G. Baets, *Adv. Photonics* **2021**, *3*, 024003.
- [36] M. Xu, M. He, H. Zhang, J. Jian, Y. Pan, X. Liu, L. Chen, X. Meng, H. Chen, Z. Li, X. Xiao, S. Yu, S. Yu, X. Cai, *Nat. Commun.* **2020**, *11*, 3911.